PHOTONICS Research

Switchable chiral mirror based on PIN diodes

Zhibiao Zhu,[1,†] [iD] Zhe Qin,[1,†] [iD] He Wang,[1] [iD] Lixin Jiang,[1] Yongfeng Li,[1,*] Wenjie Wang,[1] Hongya Chen,[1] Jiafu Wang,[1] Yongqiang Pang,[2] and Shaobo Qu[1]

[1]Shaanxi Key Laboratory of Artificially-Structured Functional Materials and Devices, Air Force Engineering University, Xi'an 710051, China
[2]School of Electronic Science and Engineering, Xi'an Jiaotong University, Xi'an 710049, China
*Corresponding author: liyf217130@126.com

Chiral mirrors can produce spin selective absorption for left-handed circularly polarized (LCP) or right-handed circularly polarized (RCP) waves. However, the previously proposed chiral mirror only absorbs the designated circularly polarized (CP) wave in the microwave frequency band, lacking versatility in practical applications. Here, we propose a switchable chiral mirror based on a pair of PIN diodes. The switchable chiral mirror has four working states, switching from the handedness-preserving mirror to the LCP mirror, RCP mirror, and perfect absorber. The basis of these advances is to change the chirality of two-dimensional (2D) chiral metamaterials and the circular conversion dichroism related to it, which is the first report in the microwave frequency band. Surface current distributions shed light on how switchable chiral mirrors work by handedness-selective excitation of reflective and absorbing electric dipole modes. Energy loss distributions verify the working mechanism. The thickness of the switchable chiral mirror is one-tenth of the working wavelength, which is suitable for integrated manufacturing. The measurement results are in good agreement with the simulation results. © 2023 Chinese Laser Press

https://doi.org/10.1364/PRJ.468496

1. INTRODUCTION

Chirality exists in natural structures and molecules, such as shells with mirror-image symmetry, DNA double helix structures, and amino acid molecules [1]. The three-dimensional (3D) chirality displayed by these biological structures is relatively weak and a challenge to improve, so applying it to practical applications is not easy. The emergence of chiral metamaterials can improve the chiral characteristics and electromagnetic (EM) response properties so that they can be used in different fields, and it can control the physical parameters of metamaterials to obtain responses in different frequency spectra [2–4]. The research on chiral metamaterials has been a significant research hotspot in the field of metamaterials, and it has unique EM and optical properties, such as asymmetric transmission [3,4], polarization conversion [5–7], circular dichroism (CD) [8,9], and chiral negative refractive index [10,11]. Meta-devices such as circular polarizers [12], broadband circular polarization converters [13], energy harvesters [14], and focusing lenses [15] have been realized.

Compared with the 3D chiral metamaterials, the planar two-dimensional (2D) chiral metamaterials have twisting characteristics, and when viewed from the opposite direction, the chirality of the 2D chiral metamaterials is precisely the opposite. Like the Archimedes spiral drawn on a transparent substrate, the spiral is reversed when viewed from the other side
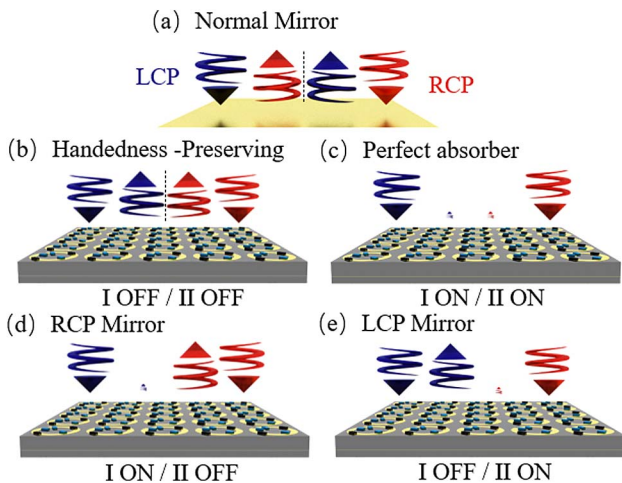
of the substrate. When planar metamaterials are under the illumination of the EM waves, whether the transmission or scattering effects depend on the twisted structure has attracted attention. Researchers have theoretically proved that planar metamaterials with this twisted structure can manipulate EM waves uniquely [16,17]. In addition, the planar structure has appeared one after another from the Greek cross fractal resonator [18], split-ring resonator [19], N-shaped resonator [20], Hilbert-shaped resonator [21], L-shaped resonator [22] to the fish-scale grid [23]. It further confirms experimentally that 2D chiral metamaterials have different rotations for left-handed circularly polarized (LCP) and right-handed circularly polarized (RCP) waves.

In recent years, chiral mirrors have been proposed to control CD, which is the differential reflection of LCP and RCP waves. Many novel designs that enhance CD have been reported and experimentally verified in the microwave and near-infrared regions. The 3D helical structure has strong inherent chirality and dipole–dipole interaction, producing large CD [24–27]. A multilayer chiral structure can create a more significant CD effect due to the interaction between layers [28,29]. In addition, a more extensive CD can be produced if a subwavelength chiral structure destroys both n-fold rotational ($n > 2$) symmetry and mirror symmetry [8]. After introducing resistance, the chiral mirror working in the microwave band can produce CD over broadband [30]. However, most chiral
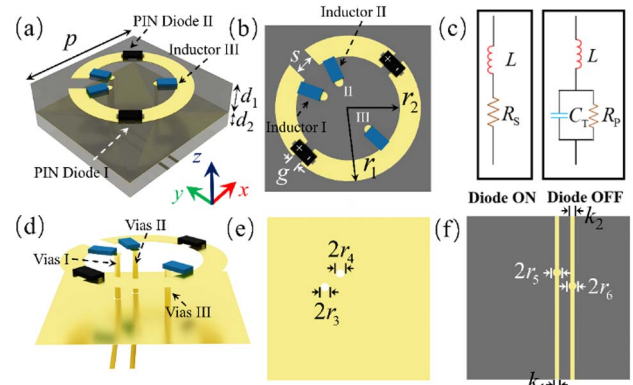
mirrors have fixed functions and can only absorb specific circularly polarized (CP) waves.

In this paper, we have experimentally proved that a switchable chiral mirror can be switched in four working states. As shown in Fig. 1, by independently controlling the ON and OFF of the two PIN diodes, we realize the electrical switching among the handedness-preserving mirror, perfect absorber, LCP mirror, and RCP mirror. Unlike using the asymmetry of the metallic pattern to achieve circular dichroism, we change the ON–OFF state of the PIN diodes to achieve distinct responses to two CP waves. When RCP and LCP waves are irradiated, stronger surface currents appear at different positions of the structure. The position of the PIN diode is determined according to this phenomenon. A switchable chiral mirror was manufactured based on the existing printed circuit board (PCB) technology, and experiments at microwave frequencies verified it. The thickness of the chiral mirror proposed in this paper is only one-tenth of the wavelength, conducive to chip integration. Such a switchable chiral mirror is highly versatile and can be applied in communications, information processing, imaging, and polarization-sensitive detection of EM waves.

The schematic diagram of the switchable chiral mirror is shown in Fig. 2. For most chiral subwavelength structures, the key to achieving circular dichroism is that the structure should simultaneously destroy n-fold ($n > 2$) rotational symmetry and mirror symmetry. Based on this principle, a split-ring resonator is proposed as a proof-of-concept to support our design. After introducing resistance on the half-arm of the metallic pattern, the symmetry of its response to EM waves can be changed through ohmic loss [30]. Reference [30] points out that the strong surface currents appear at different locations when irradiated by LCP and RCP waves. Under LCP wave illumination, the strong surface current appears on the left arm

Fig. 2. Schematic diagram of the unit cell of the switchable chiral mirror. (a) The perspective view and (b) the front view of the structure. (c) PIN diode equivalent circuit. (d) View of the Via design. Vias I and II have no contact with the intermediate metal layer, and Via III is connected to the middle metal layer. (e) The front view of the middle metallic layer. (f) The bottom feeder design. The two thin metal wires are connected to separate electrodes, respectively.

of the split ring. After introducing a resistor on the left arm of the structure, the structure can realize the strong absorption of the LCP wave, while the RCP wave is almost completely reflected. The case of RCP wave incidence is similar. The strong surface current appears on the right arm of the split ring. Thus, the split ring loaded with resistance can realize circular dichroism. Two PIN diodes are loaded on the two arms of the split-ring resonator, and the switchable chiral mirrors can be realized through the ON–OFF switching of the PIN diodes. The unit cell of the switchable chiral mirrors is analyzed and optimized by the EM simulation software CST MICROWAVE STUDIO. The optimized parameters are as follows: $p = 8$ mm, $d_1 = 2$ mm, $d_2 = 1$ mm, $r_1 = 3.5$ mm, $r_2 = 2.5$ mm, $g = 0.5$ mm, and $s = 1$ mm, as shown in Figs. 2(a) and 2(b). The switchable chiral mirror includes an upper FR4 substrate (relative dielectric constant of 4.4, loss tangent of 0.02), an intermediate metallic layer, a lower FR4 substrate, and a metallic pattern layer covering FR4. The middle homogeneous metallic layer realizes zero transmission.

As shown in Fig. 2(b), the anodes of PIN diodes I and II are on the upper side of the metallic split ring. A circuit in which the states of two PIN diodes can be independently controlled is designed. Via hole III is connected to the middle metallic layer as an electrode, and its top surface is connected to the lower end of the metallic split ring through Inductor III. Vias I and II connect the left and right sides of the opening of the metallic ring through an inductor, respectively. Vias I and II are connected to the feed lines at the bottom layer, each to a separate electrode. Figure 2(d) illustrates where Vias I and II do not directly contact the intermediate metal layer. The diameter of the copper column is 0.15 mm, $r_3 = r_4 = r_5 = r_6 = 0.2$ mm, and $k_1 = k_2 = 0.2$ mm, as illustrated in Figs. 2(e) and 2(f). The design of the round metallic gasket is to meet the needs of prototype processing and facilitate diode welding.

A suitable PIN diode (BAP70-02, NXP, Holland) [31] is selected according to the size of the switchable chiral mirror

Fig. 1. (a) Conventional mirror (metallic plate) reverses the handedness of incident CP waves. Here, we report switchable chiral mirrors that transform upon regulating voltage into (b) a handedness-preserving mirror, (c) a perfect absorber, and (d) an LCP/(e) an RCP mirror. Handedness-preserving mirrors reflect both CP waves without handedness change. In addition, the LCP/RCP mirror reflects the LCP/RCP wave without handedness reversal while absorbing the other CP waves. Moreover, the perfect absorber absorbs both LCP and RCP waves.

and the resistance value required to achieve the maximum CD. The PIN diode can be equivalent to a series connection of a small inductance ($L = 1.5$ nH) and forward resistance ($R_S = 100\ \Omega$) in the ON state. The PIN diode can be equivalent to the parallel connection of reverse resistance ($R_p = 1.5$ GΩ) and equivalent capacitance ($C_T = 0.1$ pF) in the OFF state. The small series inductance also needs to be considered in the OFF state. In one unit cell, the value of the three-chip inductors is 27 nH, and they are welded between the direct current (DC) power lines and metallic pattern as a radio frequency choke. The inductors block alternating current but allow direct current paths.

2. SIMULATION RESULTS AND ANALYSIS

The complex Jones matrix describes the incidence and reflection of electromagnetic (EM) waves passing through the metasurface. The thickness of the metasurface is much smaller than the wavelength, which can be ignored in theoretical analysis. When LCP or RCP is vertically incident, the complex amplitudes of the circular polarization incident field and reflection field can be represented by the complex Jones matrix R [32]:

$$\begin{pmatrix} r_{\text{LCP}} \\ r_{\text{RCP}} \end{pmatrix} = \begin{pmatrix} r_{LL} & r_{LR} \\ r_{RL} & r_{RR} \end{pmatrix} \begin{pmatrix} i_{\text{LCP}} \\ i_{\text{RCP}} \end{pmatrix} = R_{\text{circ}} \begin{pmatrix} i_{\text{LCP}} \\ i_{\text{RCP}} \end{pmatrix}, \quad (1)$$

where the subscript "circ" of R_{circ} means that the Jones matrix is expressed in the circular base. $r_{LL(RR)}$ and $r_{RL(LR)}$ are co- and cross-polarization reflection coefficients of the LCP (RCP) waves, respectively. The absorption for the LCP and the RCP waves of switchable chiral mirrors can be simplified as

$$A_{\text{LCP}} = 1 - |r_{RL}|^2 - |r_{LL}|^2 = 1 - R_{RL} - R_{LL}, \quad (2)$$

$$A_{\text{RCP}} = 1 - |r_{LR}|^2 - |r_{RR}|^2 = 1 - R_{LR} - R_{RR}. \quad (3)$$

For the reflection-type metasurface proposed in this paper, the CD spectrum can characterize the chirality of the structure, which describes the discrepancy between two CP waves in reflection (or absorption). The difference in reflection intensity ΔR for RCP and LCP illumination is

$$\text{CD} = \Delta R = R_{LL} - R_{RR} = A_{\text{RCP}} - A_{\text{LCP}}, \quad (4)$$

where $R_{LL} = |r_{LL}|^2$, $R_{RR} = |r_{RR}|^2$ represent the reflectivity of the LCP and the RCP waves, respectively. The PIN diode is a nonlinear device. But the proposed structure only works in four specific states. Therefore, in these specific states, Eqs. (2)–(4) are tenable. Assume that the Cartesian coordinate system is the reference coordinate system under the linear basis vector. Therefore, the relationship between the incident and reflected EM waves in the linear basis vector can be described as

$$R_{\text{lin}} = \begin{pmatrix} r_X \\ r_Y \end{pmatrix} = \begin{pmatrix} r_{xx} & r_{xy} \\ r_{yx} & r_{yy} \end{pmatrix} \begin{pmatrix} i_X \\ i_Y \end{pmatrix}. \quad (5)$$

R_{circ} can then be obtained by changing the linear-polarization bases to the circular-polarization base with the following transformation: $\vec{e}_\pm = [(\vec{x} \pm \vec{y})/\sqrt{2}] \cdot r$,

$$R_{\text{circ}} = \begin{pmatrix} r_{LL} & r_{LR} \\ r_{RL} & r_{RR} \end{pmatrix}$$
$$= \frac{1}{2} \begin{pmatrix} r_{xx} + r_{yy} + i(r_{xy} - r_{yx}) & r_{xx} - r_{yy} + i(r_{xy} + r_{yx}) \\ r_{xx} - r_{yy} - i(r_{xy} + r_{yx}) & r_{xx} + r_{yy} - i(r_{xy} - r_{yx}) \end{pmatrix}.$$
$$(6)$$

$r_{xx(yy)}$ and $r_{xy(yx)}$ represent the reflection coefficients of co- and cross-linearly polarized waves, respectively.
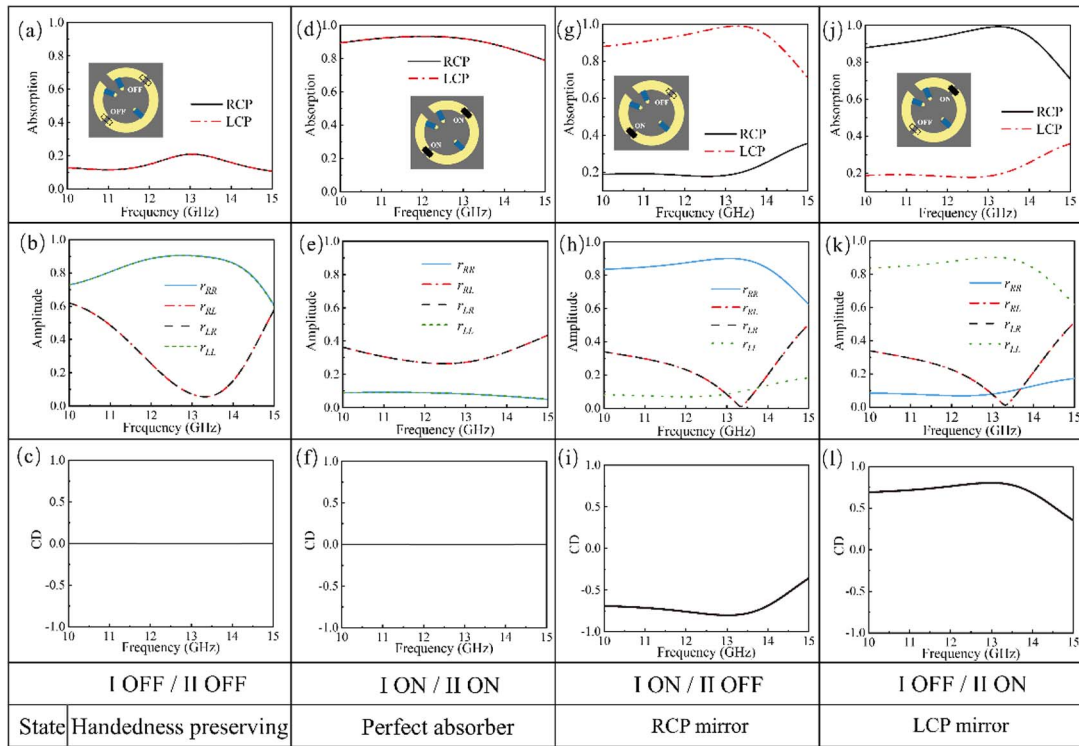
A. Handedness Preserving Mirror State

The mirror that maintains handedness for the incident CP waves with either handedness shows the same anisotropic response. Therefore, when the switchable chiral mirror is in a mirror state that maintains handedness, the structure needs to keep anisotropy. When the two PIN diodes are both in the OFF state, the chiral EM response disappears. The switchable chiral mirror becomes a handedness-preserving mirror at the working frequency (13 GHz). Figures 3(a) and 3(b) show the spectral dependence of the switchable mirror's absorption and reflectivity according to simulations when the working state is switched to the handedness preserving mirror state ($|r_{RR}|^2 \approx |r_{LL}|^2$ dominates, $|r_{RL}|^2 \approx |r_{LR}|^2$ still exists but can be ignored). The reflection matrix for circular polarization is governed by eigenvectors $u = (1/2)^{1/2}(1, i)^{\text{T}}$ and $v = (1/2)^{1/2}(1, -i)^{\text{T}}$. At the handedness preserving mirror state, the reflection coefficients must satisfy $r_{LL} = r_{RR} = 1$, $r_{RL} = r_{LR} = 0$. According to Eq. (6), the solution can be obtained with $R_{\text{lin}} = \frac{1}{2}\begin{pmatrix} 1 & 0 \\ 0 & 1 \end{pmatrix}$. The eigenvalues of $\lambda = 1$ with the eigenvectors of $(1, i)^{\text{T}}$ and $(1, -i)^{\text{T}}$ is obtained from the R_{lin}, which indicates that total reflections of LCP and RCP waves is achieved.

Our simulation reveals the physical origin of the chirality-maintaining mirror state, which shows how the incident LCP and RCP interact with a split resonant ring loaded with two PIN diodes at 13 GHz. The current distribution on the metallic pattern surface has been studied and shown in Figs. 4(a) and 4(b). The redder the arrow color, the stronger the surface current. The surface currents induced on the metallic surface are weak under the irradiation of the LCP and the RCP waves. At this working state, the energy loss distributions of the structure show the same results, as shown in Figs. 5(a) and 5(b). The directions of the electric dipoles excited by the RCP and LCP waves are the same. The electric dipole effectively radiates, causing near-complete circular conversion ($|r_{LL}|^2$ and $|r_{RR}|^2$, respectively) and generating a counter-rotating field that is different from the incident CP wave. It is worth mentioning that the two PIN diodes are both in the OFF state, and the energy of the incident EM wave is almost not lost. At the handedness preserving mirror state, the value of the CD is zero at the working frequency band [as shown in Fig. 3(c)].

B. Perfect Absorber State

When both PIN diodes are conducting, the switchable chiral mirror can be switched to the absorber state. At 13 GHz, the absorption rate of the absorber is above 90%. Both LCP and RCP waves are almost fully absorbed at their working frequency band through the ohmic loss of two PIN diodes.

Fig. 3. Simulated (a) absorption spectra, (b) reflection amplitudes ($|r|$), and (c) CD spectra of the handedness preserving mirror state (PIN diode I OFF, PIN diode II OFF) at normal incidence. Simulated (d) absorption spectra, (e) reflection amplitudes, and (f) CD spectra of the perfect absorber state (PIN diode I ON, PIN diode II ON) at normal incidence. Simulated (g) absorption spectra, (h) reflection amplitudes, and (i) CD spectra of the RCP mirror state (PIN diode I ON, PIN diode II OFF) at normal incidence. Simulated (j) absorption spectra, (k) reflection amplitudes, and (l) CD spectra of the LCP mirror state (PIN diode I OFF, PIN diode II ON) at normal incidence.

Figures 3(d) and 3(e) show the simulated absorption and reflectivity of the absorber when PIN diodes I and II are in the ON state. At the absorber state, the reflection coefficients must satisfy $r_{LL} = r_{RR} = r_{RL} = r_{LR} = 0$. According to Eq. (6),
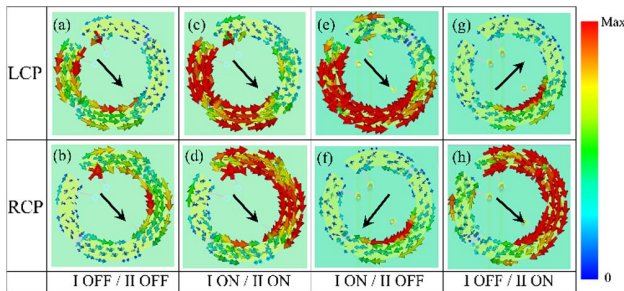
Fig. 4. The surface current distributions of the switchable chiral mirror at the handedness preserving mirror state under the normal incidence of (a) LCP and (b) RCP waves at 13 GHz, respectively. The surface current distributions of the switchable chiral mirror at the absorber state under the normal incidence of (c) LCP and (d) RCP waves at 13 GHz, respectively. The surface current distributions of the switchable chiral mirror at the RCP mirror state under the normal incidence of (e) LCP and (f) RCP waves at 13 GHz, respectively. The surface current distributions of the switchable chiral mirror at the LCP mirror state under the normal incidence of (g) LCP and (h) RCP waves at 13 GHz, respectively. Arrows indicate electric dipoles corresponding to resonant currents excited by the CP waves of opposite handedness.

the solution can be obtained with $R_{\text{lin}} = \frac{1}{2}\begin{pmatrix} 0 & 0 \\ 0 & 0 \end{pmatrix}$. The eigenvalues of $\lambda = 1$ with the eigenvectors of $(1, i)^{\text{T}}$ and $(1, -i)^{\text{T}}$ are obtained from the R_{lin}, which indicates that total absorption of the LCP and the RCP waves is achieved.

Our simulation reveals the physical origin of the absorber state, which shows how the incident LCP and RCP interact with the split resonant ring loaded with two PIN diodes at 13 GHz. In this working state, the current on the surface of the metallic pattern is stronger under the incidence of two CP waves. Figures 4(c) and 4(d) show the instantaneous distribution of the surface current. In fact, we observed in the animation of surface current that a strong surface current oscillates back and forth on the left arm of the split ring under LCP wave irradiation. The LCP wave excites strong electric dipole. The strong currents just go through the PIN diode on the left arm. The diode is in a conducting state ($R_{\text{ON}} = 100\ \Omega$), resulting in a large loss of EM waves. Notably, the current on the right arm is weak under LCP illumination. Under the irradiation of the RCP wave, a strong current oscillates back and forth on the right arm of the split ring, and the analysis is similar to that of the LCP wave. As a verification, the energy loss distributions are provided in Figs. 5(c) and 5(d), which show that under the incidence of the LCP and the RCP waves, the location where the loss occurs is different. At the perfect absorber state, the value of the CD is zero at the working frequency band [as shown in Fig. 3(f)].
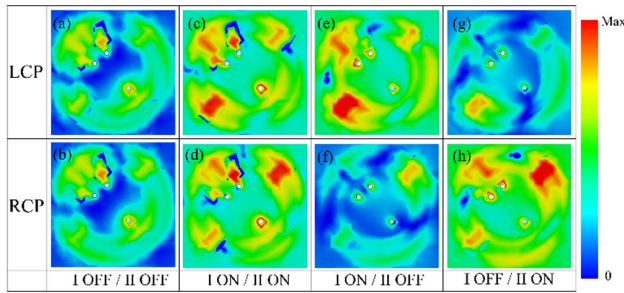
Fig. 5. The energy loss distributions on the structure surface at the handedness preserving mirror state under the normal incidence of (a) LCP and (b) RCP waves at 13 GHz, respectively. The energy loss distributions on the structure surface at the absorber state under the normal incidence of (c) LCP and (d) RCP waves at 13 GHz, respectively. The energy loss distributions on the structure surface at the RCP mirror state under the normal incidence of (e) LCP and (f) RCP waves at 13 GHz, respectively. The energy loss distributions on the structure surface at the LCP mirror state under the normal incidence of (g) LCP and (h) RCP waves at 13 GHz, respectively.

C. RCP Mirror State

The split-ring resonator proposed in this paper is loaded with PIN diodes to change the symmetry of the structure's response to two CP waves. When PIN diode I is in the ON state and

PIN diode II is in the OFF state, the state of the chiral mirror is switched to the RCP mirror. At its resonance ($f = 13$ GHz), the RCP wave intensity is almost fully reflected without handedness change ($|R_{RR}|^2$), while the LCP wave is almost fully absorbed through the ohmic loss of PIN diode I. Figures 3(g) and 3(h) show the simulated structure's absorption and reflectivity at the RCP mirror state. At the RCP mirror state, the reflection coefficients must satisfy $r_{LL} = r_{LR} = r_{RL} = 0$, $r_{RR} = 1$. According to Eq. (6), the solution can be obtained with $R_{\text{lin}} = \frac{1}{2}\begin{pmatrix} 1 & i \\ -i & 1 \end{pmatrix}$. The eigenvalue of $\lambda_1 = 0$ with the eigenvector of $(1, i)^{\text{T}}$ indicates that total absorption of LCP is achieved, and the eigenvalue of $\lambda_2 = 1$ with the eigenvector of $(1, -i)^{\text{T}}$ indicates that total reflection of RCP is achieved.

Our simulation reveals the physical mechanism behind the RCP mirror. The distribution of the surface current and the energy loss can directly analyze the cause of the CD generation of the switchable chiral mirror at the RCP mirror state. The RCP mirror response is caused by the two linear electric dipoles excited by LCP and RCP [Figs. 4(e) and 4(f)]. Under the irradiation of the LCP wave, strong surface currents oscillate back and forth on the left arm of the split ring and form a strong electric dipole. The PIN diode on the left arm is ON ($R_{\text{ON}} = 100\ \Omega$), which results in a large loss of the LCP wave. Meanwhile, the surface current on the right arm of the split ring
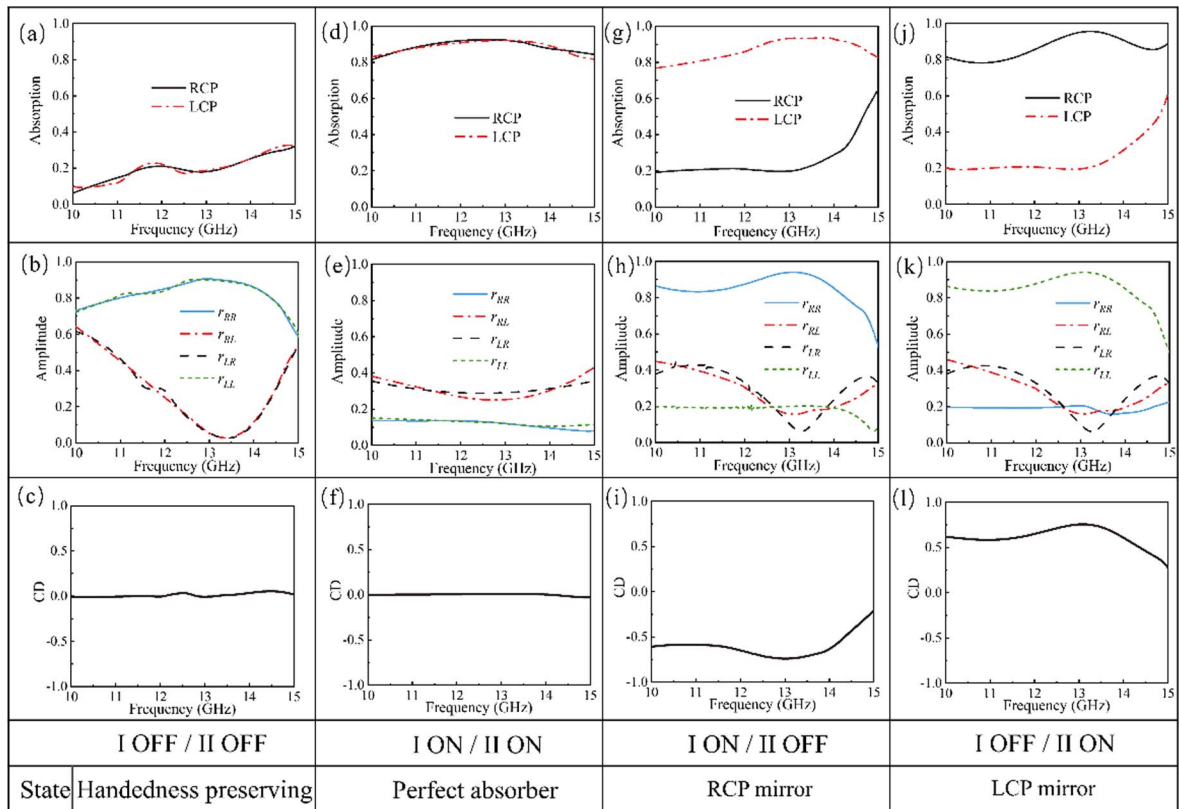
Fig. 6. Measured (a) absorption spectra, (b) reflection amplitudes, and (c) CD spectra of the handedness preserving mirror state at normal incidence. Measured (d) absorption spectra, (e) reflection amplitudes, and (f) CD spectra of the perfect absorber state at normal incidence. Measured (g) absorption spectra, (h) reflection amplitudes, and (i) CD spectra of the RCP mirror state at normal incidence. Measured (j) absorption spectra, (k) reflection amplitudes, and (l) CD spectra of the LCP mirror state at normal incidence.

is weak, forming a weak electric dipole. The PIN diode of the right arm is in the OFF state, so the RCP wave is almost not lost. The distribution of energy loss in the RCP mirror state verifies the above derivation [as shown in Figs. 5(e) and 5(f)]. The different energy losses result in the absorption of the structure under the LCP wave incidence being larger than that under the RCP wave. At the RCP mirror state, the sign of the CD is negative at the working frequency band [as shown in Fig. 3(i)].

It is necessary to explain why the electric dipole mode can cause a nearly perfect reflection of the RCP. The ideal linear electric dipole radiates linear polarization, that is, the superposition of equal-strength fields with opposite handedness. The fields radiated along $-z$ and $+z$ rotating together with the incident field can (destructively) interfere with the incident field (along $-z$) and with its reflection by the metal backing plate (along $+z$). In this way, the field rotating in the same direction as the incident disappears in the structure at the RCP mirror state. The radiation field rotating in the opposite direction compared with the incident field still exists (circular polarization conversion). These counter-rotating incident and reflected fields have the same circular polarization when propagating in the opposite direction, which means that their handedness must be evaluated by an observer looking from the opposite direction.

D. LCP Mirror State

In order to realize a chiral mirror with opposite handedness, a diode configuration with opposite circular conversion dichroism is required. Therefore, compared to the RCP mirror, it is necessary to reverse the ON–OFF configuration of the two PIN diodes to convert the chiral mirror to the opposite handedness. When the diode loaded on the left arm is in the OFF state, and the diode on the right arm is in the ON state, the state of the chiral mirror is switched to the RCP mirror state. At its resonance ($f = 13$ GHz), the LCP intensity is almost fully reflected without a chiral change ($|R_{LL}|^2$), while RCP is almost fully absorbed through the ohmic loss of PIN diode II [Figs. 3(j) and 3(k)]. This phenomenon corresponds to a nearly perfect CD conversion, where ΔR_L is almost unity. At the LCP mirror state, the reflection coefficients must satisfy $r_{RR} = r_{LR} = r_{RL} = 0$, $r_{LL} = 1$. According to Eq. (6), the solution can be obtained with $R_{\text{lin}} = \frac{1}{2}\begin{pmatrix} 1 & -i \\ i & 1 \end{pmatrix}$. The eigenvalue of $\lambda_1 = 0$ with the eigenvector of $(1, -i)^{\text{T}}$ indicates that total absorption of RCP is achieved. The eigenvalue of $\lambda_2 = 1$ with the eigenvector of $(1, i)^{\text{T}}$ indicates that total reflection of LCP is achieved.

The physical origin of the LCP mirror is revealed by simulating the excitation mode of the incident LCP and RCP through the chiral resonance of the structure. This part of the analysis is the same as the RCP mirror. The electric dipole excitation is induced by LCP [Fig. 4(g)], which leads to a nearly complete circular conversion ($|R_{LL}|^2$). Under RCP wave illumination, strong surface currents oscillate back and forth on the right arm of the split ring, and a strong electric dipole is excited [Fig. 4(h)]. The PIN diode on the right arm is ON ($R_{\text{ON}} = 100\ \Omega$), and a strong surface current passes through the diode, resulting in complete absorption of the RCP wave.

In the working state of the LCP mirror, the value of the CD is positive.

3. EXPERIMENTAL RESULTS

Figure 6 shows experimental results, which are in good agreement with the simulation results. As shown in Fig. 7, a prototype of the switchable chiral mirror was manufactured and measured to verify the simulation. The prototype includes 25×25 unit cells arranged in the same direction with a total area of $200\ \text{mm} \times 210\ \text{mm}$, and four DC power lines are etched on the four sides of the panel. Two BAP 70-02 PIN diodes and three 27 nH chip inductors with a package of 1.6×0.8 mm are soldered on each unit cell. According to the datasheet of the diode, the operating power range of the PIN diode is 0–0.02 W. The voltages on the periphery of the prototype are V_1 and V_2, which control the states of all PIN diodes I and II, respectively. V_1 and V_2 are provided by feeders I and II, respectively. When $V_1 = 0$ V and $V_2 = 0$ V, the state of the switchable chiral mirror can be switched to the handedness preserving mirror state. When $V_1 = 0$ V and $V_2 = +1$ V, the state of the switchable chiral mirror can be switched to the LCP mirror state. When $V_1 = +1$ V and $V_2 = 0$ V, the state of the switchable chiral mirror can be switched to the RCP mirror state. The state of the switchable chiral mirror can be switched to the perfect absorber state when $V_1 = +1$ V and $V_2 = +1$ V. The frequency
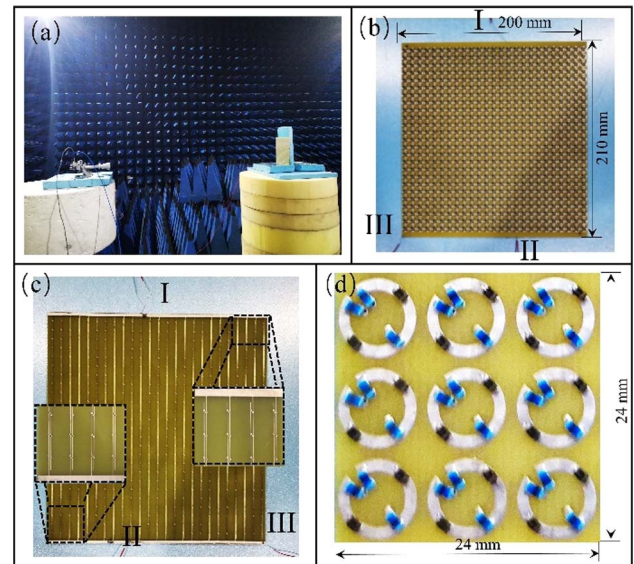
Fig. 7. Photograph of the switchable chiral mirror prototype. (a) The measurement system, (b) the front view, and (c) the back view. All Vias I in a row are connected in a series on the backside of the dielectric substrate and connected to the top metal patch (not connected to the bottom metal patch). Feeder I provides voltage V_1. All Vias II in a row are connected in a series on the backside of the dielectric substrate to connect to the bottom metal patch (without connecting to the top metal patch). Feeder II provides voltage V_2. A separate Via in the lower right corner connects to the ground Via feeder III. It is worth noting that the metal backplane is in the middle layer, connected to feeder III through the Via in the lower right corner. (d) The local view.

band of one pair of CP horn antennas used is 8–15 GHz. In the measurement, one CP horn antenna acts as a transmitter, the other acts as a receiver, and they are connected to a vector network analyzer (VNA). The prototype of the switchable chiral mirror is fixed at the same height as the CP horn antenna. The discrepancies between the measured and simulated results are uncertainty in parasitic element values, the manufacturing error of the PCB board, and the measurement error.

4. CONCLUSION

In summary, we introduced a pair of PIN diodes to realize a switchable chiral mirror capable of producing selective spin absorption. It can work in four working states by changing the state of the PIN diode. When one PIN diode turns ON and one PIN diode turns OFF, simulation and measurement prove that both the LCP and RCP mirrors can produce a significant CD difference. These functions can be traced back to the excitation of the electric dipole modes by the incident LCP and RCP. Surface current and energy loss distributions illustrate different chiral properties under different working conditions. Our switchable chiral mirror can be used to actively control the reflection, absorption, and polarization of EM waves in the microwave region. Our work has opened up a new way to design circular dichroic microwave devices and has broad application prospects in designing multifunctional components.

Disclosures. The authors declare no conflicts of interest.

Data Availability. The datasets presented in this paper are available from the corresponding author upon reasonable request.

†These authors contributed equally to this paper.

REFERENCES

1. L. D. Barron, *Molecular Light Scattering and Optical Activity*, 2nd ed. (Cambridge University, 2004).
2. V. A. Fedotov, P. L. Mladyonov, S. L. Prosvirnin, A. V. Rogacheva, Y. Chen, and N. I. Zheludev, "Asymmetric propagation of electromagnetic waves through a planar chiral structure," Phys. Rev. Lett. **97**, 167401 (2006).
3. R. Singh, E. Plum, C. Menzel, C. Rockstuhl, A. K. Azad, R. A. Cheville, F. Lederer, W. Zhang, and N. I. Zheludev, "Terahertz metamaterial with asymmetric transmission," Phys. Rev. B **80**, 153104 (2009).
4. A. S. Schwanecke, V. A. Fedotov, V. V. Khardikov, S. L. Prosvirnin, Y. Chen, and N. I. Zheludev, "Nanostructured metal film with asymmetric optical transmission," Nano Lett. **8**, 2940–2943 (2008).
5. H. Y. Chen, J. F. Wang, H. Ma, S. B. Qu, Z. Xu, A. X. Zhang, M. B. Yan, and Y. F. Li, "Ultra-wideband polarization conversion metasurfaces based on multiple plasmon resonances," J. Appl. Phys. **115**, 154504 (2014).
6. M. Feng, J. Wang, H. Ma, W. Mo, H. Ye, and S. Qu, "Broadband polarization rotator based on multi-order plasmon resonances and high impedance surfaces," J. Appl. Phys. **114**, 074508 (2013).
7. Y. Li, J. Zhang, S. Qu, J. Wang, L. Zheng, Y. Pang, Z. Xu, and A. Zhang, "Achieving wide-band linear-to-circular polarization conversion using ultra-thin bi-layered metasurfaces," J. Appl. Phys. **117**, 044501 (2015).
8. Z. Wang, H. Jia, K. Yao, W. Cai, H. Chen, and Y. Liu, "Circular dichroism metamirrors with near-perfect extinction," ACS Photon. **3**, 2096–2101 (2016).
9. H. Wang, Z. Qin, L. Huang, Y. Li, R. Zhao, H. Zhou, H. He, J. Zhang, and S. Qu, "Metasurface with dynamic chiral meta-atoms for spin multiplexing hologram and low observable reflection," PhotoniX **3**, 10 (2022).
10. M. Li, J. Song, and F. Wu, "Ultra-compact chiral metamaterial with negative refractive index based on miniaturized structure," J. Magn. Magn. Mater. **426**, 150–154 (2017).
11. J. Dong, J. Zhou, T. Koschny, and C. Soukoulis, "Bi-layer cross chiral structure with strong optical activity and negative refractive index," Opt. Express **17**, 14172–14179 (2009).
12. R. Jie, H. Jing, S. Li, and Y. Xiao, "Dual-band circular polarizers based on a planar chiral metamaterial structure," IEEE Antennas Wireless Propag. Lett. **18**, 2587–2591 (2019).
13. Y. Jing, Y. Li, J. Zhang, J. Wang, M. Feng, T. Qiu, H. Wang, Y. Han, H. Ma, and S. Qu, "Achieving circular-to-linear polarization conversion and beam deflection simultaneously using anisotropic coding metasurfaces," Sci. Rep. **9**, 12264 (2019).
14. O. M. Ramahi, T. S. Almoneef, M. Alshareef, and M. S. Boybay, "Metamaterial particles for electromagnetic energy harvesting," Appl. Phys. Lett. **101**, 173903 (2012).
15. A. Pors, M. G. Nielsen, R. L. Eriksen, and S. I. Bozhevolnyi, "Broadband focusing flat mirrors based on plasmonic gradient metasurfaces," Nano Lett. **13**, 829–834 (2013).
16. A. V. Krasavin, A. S. Schwanecke, and N. I. Zheludev, "Extraordinary properties of light transmission through a small chiral hole in a metallic screen," J. Opt. A **8**, S98–S105 (2006).
17. M. Reichelt, S. W. Koch, A. V. Krasavin, J. V. Moloney, A. S. Schwanecke, T. Stroucken, E. M. Wright, and N. I. Zheludev, "Broken enantiomeric symmetry for electromagnetic waves interacting with planar chiral nanostructures," Appl. Phys. B **84**, 97–101 (2006).
18. R. Zhao, L. Zhang, J. Zhou, Th. Koschny, and C. M. Soukoulis, "Conjugated gammadion chiral metamaterial with uniaxial optical activity and negative refractive index," Phys. Rev. B **83**, 035105 (2011).
19. E. Plum and N. I. Zheludev, "Chiral mirrors," Appl. Phys. Lett. **106**, 221901 (2015).
20. Q. Zheng, Y. Li, J. Zhang, H. Ma, J. Wang, Y. Pang, Y. Han, S. Sui, Y. Shen, H. Chen, and S. Qu, "Wideband, wide-angle coding phase gradient metasurfaces based on Pancharatnam-Berry phase," Sci. Rep. **7**, 43543 (2017).
21. H. M. Xu, G. M. Wang, M. Q. Qi, T. Cai, and T. J. Cui, "Compact dual-band circular polarizer using twisted Hilbert-shaped chiral metamaterial," Opt. Express **21**, 24912–24921 (2013).
22. V. A. Fedotov, A. S. Schwanecke, N. I. Zheludev, V. V. Khardikov, and S. L. Prosvirnin, "Asymmetric transmission of light and enantiomerically sensitive plasmon resonance in planar chiral nanostructures," Nano Lett. **7**, 1996–1999 (2007).
23. C. Wu, N. Arju, G. Kelp, J. A. Fan, J. Dominguez, E. Gonzales, E. Tutuc, I. Brener, and G. Shvets, "Spectrally selective chiral silicon metasurfaces based on infrared Fano resonances," Nat. Commun. **5**, 3892 (2014).
24. J. Hu, X. Zhao, R. Li, A. Zhu, L. Chen, Y. Lin, B. Cao, X. Zhu, and C. Wang, "Broadband circularly polarizing dichroism with high efficient plasmonic helical surface," Opt. Express **24**, 11023–11032 (2016).
25. M. Schäferling, X. Yin, N. Engheta, and H. Giessen, "Helical plasmonic nanostructures as prototypical chiral near-field sources," ACS Photon. **1**, 530–537 (2014).
26. Y. Yu, Z. Yang, S. Li, and M. Zhao, "Higher extinction ratio circular polarizers with hetero-structured double-helical metamaterials," Opt. Express **19**, 10886–10894 (2011).
27. Z. Fan and A. O. Govorov, "Plasmonic circular dichroism of chiral metal nanoparticle assemblies," Nano Lett. **10**, 2580–2587 (2010).
28. L. Wu, Z. Yang, Y. Cheng, Z. Lu, P. Zhang, M. Zhao, R. Gong, X. Yuan, Y. Zheng, and J. Duan, "Electromagnetic manifestation of

chirality in layer-by-layer chiral metamaterials," Opt. Express **21**, 5239–5246 (2013).

29. X. Yin, M. Schaferling, B. Metzger, and H. Giessen, "Interpreting chiral nanophotonic spectra: the plasmonic Born–Kuhn model," Nano Lett. **13**, 6238–6243 (2013).

30. M. Feng, X. Chen, Y. Li, Q. Zheng, Y. Han, J. Zhang, J. Wang, Y. Hou, Z. Liu, X. Li, C. Wang, J. Jing, H. Ma, and S. Qu, "Circularly polarized spin-selectivity absorbing coding phase gradient metasurface for RCS reduction," Adv. Theory Simul. **3**, 1900217 (2020).

31. NXP Semiconductors, 2020, https://www.alldatasheetcn.com/datasheetpdf/pdf/468426/NXP/BAP70-02.html.

32. Y. Li, Y. Pang, J. Wang, Q. Zheng, L. Zheng, M. Feng, Y. Jing, J. Zhang, T. Cui, and S. Qu, "Bispectral circular dichroic coding metasurfaces," Ann. Phys. **532**, 1900496 (2020).